Solar absorption by elemental and brown carbon determined from spectral observations

Ranjit Bahadur, Puppala S. Praveen, Yangyang Xu, and V. Ramanathan[1]

Scripps Institution of Oceanography, University of California at San Diego, La Jolla, CA 92093-0221

Edited by Mark H. Thiemens, University of California at San Diego, La Jolla, CA, and approved September 11, 2012 (received for review April 9, 2012)

Black carbon (BC) is functionally defined as the absorbing component of atmospheric total carbonaceous aerosols (TC) and is typically dominated by soot-like elemental carbon (EC). However, organic carbon (OC) has also been shown to absorb strongly at visible to UV wavelengths and the absorbing organics are referred to as brown carbon (BrC), which is typically not represented in climate models. We propose an observationally based analytical method for rigorously partitioning measured absorption aerosol optical depths (AAOD) and single scattering albedo (SSA) among EC and BrC, using multiwavelength measurements of total (EC, OC, and dust) absorption. EC is found to be strongly absorbing (SSA of 0.38) whereas the BrC SSA varies globally between 0.77 and 0.85. The method is applied to the California region. We find TC (EC + BrC) contributes 81% of the total absorption at 675 nm and 84% at 440 nm. The BrC absorption at 440 nm is about 40% of the EC, whereas at 675 nm it is less than 10% of EC. We find an enhanced absorption due to OC in the summer months and in southern California (related to forest fires and secondary OC). The fractions and trends are broadly consistent with aerosol chemical-transport models as well as with regional emission inventories, implying that we have obtained a representative estimate for BrC absorption. The results demonstrate that current climate models that treat OC as nonabsorbing are underestimating the total warming effect of carbonaceous aerosols by neglecting part of the atmospheric heating, particularly over biomass-burning regions that emit BrC.

short lived climate pollutants | aerosol forcing

Black carbon (BC) emitted from combustion sources such as automobile exhaust and biomass burning (1–3) absorbs solar radiation in both the visible and the near-infrared spectra and is estimated to be a principal contributor to global atmospheric warming (4). The short atmospheric lifetime of BC aerosol particles, typically of the order of 1 wk (5, 6), compared with greenhouse gases (which have atmospheric lifetimes of several years or decades) results in BC being not well mixed in the atmosphere but instead geographically and temporally correlated to emission sources. For this reason, reducing BC emissions is an attractive control strategy for climate change that is expected to have a more immediate and regional impact (4, 7, 8). The state of California appears to be a successful example where aggressive control policies for vehicular diesel emissions and domestic wood burning have produced a near 50% decrease in BC concentrations (9). This decline in conjunction with the near-static concentrations of primarily scattering aerosol particles (such as sulfates) may have led to a large negative change in the direct radiative forcing (9).

A simplification in such model estimates of aerosol forcing is that BC is considered to be equivalent to elemental carbon (EC), and the organic fraction of carbonaceous aerosols [organic carbon (OC)] is treated as scattering and is therefore found to have a cooling impact on the climate (10, 11). It is important to realize not only that BC from all emission sources contains both elemental and organic fractions (12), but also that nonsoot OC, particularly that emitted from biomass burning processes, has a significant absorbing component at short wavelengths that may be comparable to the EC absorption (13–17). Consequently, OC that is weakly absorbing in the visible and near-UV spectra may also contribute to the warming potential of aerosols. In addition to their differing spectral dependence, the wide range of optical properties reported for EC, OC, and mineral dust in the literature (18–22) leads to uncertainties in estimating the absorption attributable to these species. Whereas the attribution of ambient aerosol absorption to EC may be a reasonable approximation in areas dominated by fresh soot emissions, it may lead to misleading estimates of the aerosol forcing when other light-absorbing particles are present.

In more complex environments, a separation of the total absorption into different chemical species is therefore essential, both for constraining the large uncertainties in current aerosol-forcing estimates (23) and for informing any emissions-based control policy. Recent studies reporting the fractions of EC, OC, and mineral dust absorption follow one of three general approaches. First, measured optical and size distribution properties of the aerosol are related to spatial emission patterns to determine the dominant absorbing species (24–27); second, detailed aerosol transport and chemistry models are used in conjunction with assumed optical properties to estimate absorption that is validated against measurements (28–33); and third, closure studies are performed to relate collocated chemically resolved measurements of aerosol mass with optical measurements (34, 35). A recent study by Chung et al. (36) exploited the wavelength dependence of the absorption aerosol optical depths (AAOD) of BC, brown carbon (BrC), and dust aerosols to resolve their relative contribution to the observed absorption optical depths, but used published values for the wavelength dependence of AAOD for OC (brown carbon) and assumed the single scattering albedo (SSA) for EC and OC instead of self-consistently determining these critical properties from observations. This study uses the formalism of Chung et al. without invoking the assumptions noted above. Specifically, the present approach offers the following major improvements: (*i*) By solving for BC and BrC simultaneously we eliminate the need for assumption of total carbonaceous aerosol (TC) properties that depend on source-specific compositions. (*ii*) The OC AAE is determined empirically by exploiting measurements at the longer wavelengths of 870 and 1020 nm. (*iii*) We consider scattering optical depths to better constrain the phase space on the basis of size. (*iv*) Finally, we also offer empirical estimates of the SSA. The proposed empirical scheme requires only a single set of aerosol optical measurements, allowing for spatial and temporal coverage on a nearly global scale. We provide a robust set of constraints that will allow climate modelers to improve the estimation of the BrC aerosol forcing.

The remainder of this paper is organized as follows: We describe the equations composing our partitioning scheme; the

Author contributions: V.R. designed research; R.B., P.S.P., Y.X., and V.R. performed research; R.B. contributed new reagents/analytic tools; R.B., P.S.P., and Y.X. analyzed data; and R.B. wrote the paper.

The authors declare no conflict of interest.

This article is a PNAS Direct Submission.

[1]To whom correspondence should be addressed. E-mail: vramanathan@ucsd.edu.

This article contains supporting information online at www.pnas.org/lookup/suppl/doi:10.1073/pnas.1205910109/-/DCSupplemental.

equations are parameterized using an observational dataset as input; the scheme uses observations from California as a test case to determine EC, OC, and dust absorption; our estimates are compared with model predictions and emission inventories; and finally we comment on the limitations of our scheme and the scope for future applications.

Partitioning AAOD

The total aerosol optical depth (AOD) represents the total light extinction due to scattering and absorption by an aerosol and is related to the AAOD through the SSA as

$$\mathrm{AAOD}(\lambda) = (1 - \mathrm{SSA}(\lambda)) \times \mathrm{AOD}(\lambda). \quad [1]$$

The AOD and AAOD are extensive properties that depend on the total aerosol concentration, whereas the SSA (the fraction of total aerosol extinction due to scattering) is an intensive property that depends only on the aerosol composition; however, the value of all three depends on the wavelength of the incident light. The spectral dependence of the AOD and AAOD is related to reference values with an exponential dependence

$$\mathrm{AOD}(\lambda) = \mathrm{AOD}_{\mathrm{ref}} \left(\lambda/\lambda_{\mathrm{ref}}\right)^{-\mathrm{EAE}}$$

$$\mathrm{AAOD}(\lambda) = \mathrm{AAOD}_{\mathrm{ref}} \left(\lambda/\lambda_{\mathrm{ref}}\right)^{-\mathrm{AAE}}. \quad [2]$$

In the classical formulation, the extinction angstrom exponent (EAE) and absorption angstrom exponent (AAE) are thought to be constants; however, recent studies have shown them to depend on the wavelength, particle size, and particle composition (37–39). Because the total AAOD is an extensive property, the contributions due to EC, OC, and dust are additive such that

$$\mathrm{AAOD}(\lambda) = \mathrm{AAOD}_{\mathrm{EC}}(\lambda) + \mathrm{AAOD}_{\mathrm{OC}}(\lambda) + \mathrm{AAOD}_{\mathrm{dust}}(\lambda). \quad [3]$$

Eqs. **2** and **3** can be combined to generate a set of independent equations that compose our primary formulation:

$$\begin{aligned}\mathrm{AAOD}(\lambda_i) = {} & \mathrm{AAOD}_{\mathrm{ref,EC}} \left(\lambda_i/\lambda_{\mathrm{ref}}\right)^{-\mathrm{AAEEC},i} \\ & + \mathrm{AAOD}_{\mathrm{ref,OC}} \left(\lambda_i/\lambda_{\mathrm{ref}}\right)^{-\mathrm{AAEOC},i} \\ & + \mathrm{AAOD}_{\mathrm{ref,dust}} \left(\lambda_i/\lambda_{\mathrm{ref}}\right)^{-\mathrm{AAEdust},i}.\end{aligned} \quad [4]$$

If the AAOD is known in at least three wavelengths (i.e., $i = 1, 2, 3$), the three-part Eq. **4** can be solved for the three unknown reference AAOD values corresponding to EC, OC, and dust, which can then in turn be used to partition the AAOD at any wavelength (Fig. S4). The complete set of AAE values parameterizes these equations and constrains the phase space in which physically relevant solutions exist. There are only two inherent assumptions in this formulation: First, the AAE values for the component absorbing species EC, OC, and dust are intrinsic properties that are not dependent on the mixing state; and second, the measured AAOD value represents a well-mixed sample of these species.

The full implementation of this method requires knowledge of the AAE values to partition the AAOD and of the SSA values to determine the AOD. In theory a number of pathways can be used to determine these parameters, but as stated in the introductory section, in this work we rely only on empirical values derived from optical measurements of ambient aerosols. Finally, because the absorption and scattering components of extinction can be related to aerosol chemistry and size, respectively (40), we use the scattering angstrom exponent (SAE) in place of the EAE for the remainder of this work.

The ground-based Aerosol Robotic Network (AERONET), a globally distributed network of automated sun and sky radiometers (41), provides long-term, continuous, and readily available measurements of aerosol optical properties that are an ideal resource for this study. In addition to multiband retrievals of AOD between 340 and 1,020 nm from direct sun measurements, the inversion algorithm provides SSA (and corresponding AAOD) estimates from sky radiance measurements at 440, 675, 870, and 1020 nm (42).

Absorption Angstrom Exponent

Because the primary focus of this work is partitioning absorption in the visible and near-UV spectra, we select the three shortest AERONET wavelengths for the remainder of our analysis. We designate the angstrom exponents for AOD and AAOD between 440 and 675 nm as SAE1 and AAE1 and similarly the angstrom exponents between 675 and 870 nm as SAE2 and AAE2, respectively.

Several AERONET sites are dominated by emissions corresponding to a single absorbing aerosol (25). To determine the angstrom exponents and SSA for the pure species in Eq. **4**, we have selected sites typically dominated by specific sources related to dust, EC, and OC with details in Table S1. In addition to providing

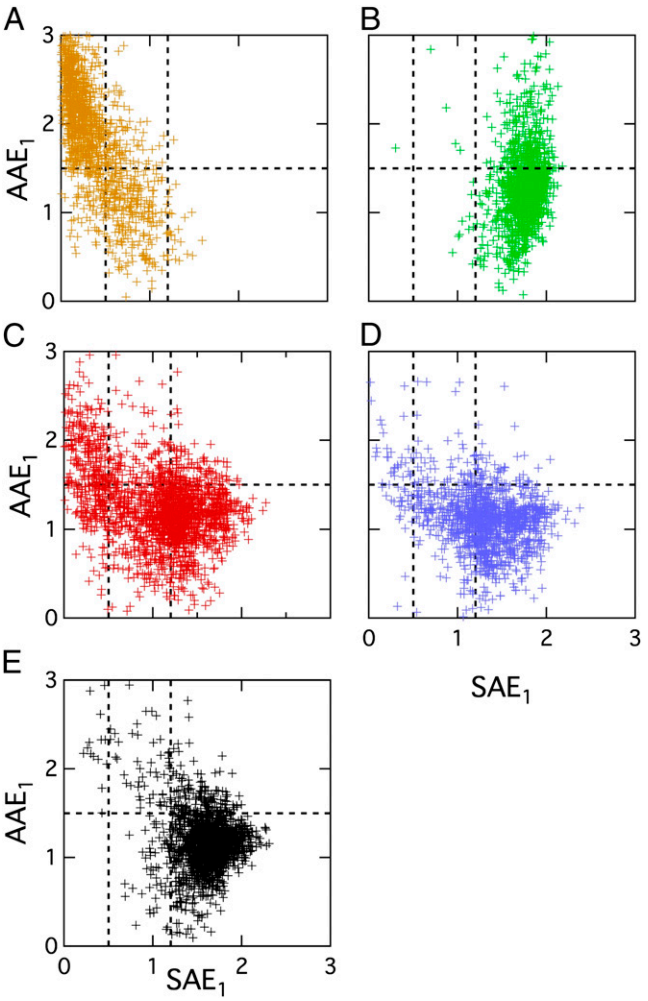

Fig. 1. (*A–E*) Scatter plots of AAE1 and SAE1 calculated from AERONET measurements at (*A*) dust (DU), (*B*) BB, (*C*) UF, (*D*) NF, and (*E*) CA sites. Dashed lines illustrate the threshold values of SAE1 = 0.5, SAE1 = 1.2, and AAE1 = 1.5 used to separate dust-dominated and dust-free regimes.

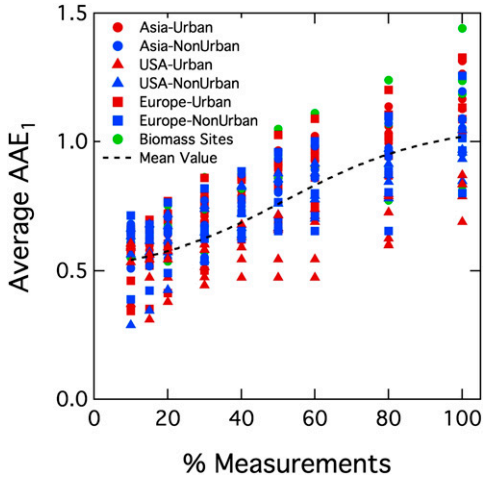

Fig. 2. Mean value of AAE1 determined by averaging the frequency distribution for AERONET sites in Table S1. The dashed line shows a fit to the mean value.

insights into pure component properties, the varying geographic location and sources associated with these sites allow us to test our hypothesis that AAE and SSA are intrinsic properties.

Dust aerosols have a crustal origin distinct from the combustion-related origin of carbonaceous aerosols and have been shown to have significantly different wavelength dependences of absorption and scattering (25), allowing us to establish thresholds in AAE1 and SAE1 for identifying dust-dominated and dust-free measurements. We provide the detailed analysis and corresponding figures in *SI Text*. Measurements with SAE1 < 0.5 are found to be dust dominated and for pure mineral dust we find AAE1 = 2.20 ± 0.50 and AAE2 = 1.15 ± 0.40. The conditions SAE1 > 1.2 or AAE2/AAE1 > 0.8 correspond to dust-free (alternatively, carbon-dominated) measurements (Fig. S1) and AAE1 calculated for total carbon is found to be 1.06 [nonurban fossil fuel (NF)], 1.14 [urban fossil fuel (UF)], and 1.28 [biomass burning (BB)], agreeing well with the value of 1.0 typically reported for BC (20). It is important to note two subtle yet important conclusions based on these values. First, the similarity in magnitude across varied geographical regions and emission sources (Figs. S3 and S4) supports the hypothesis that the absorption angstrom exponent is an inherent intrinsic property. Second, the differences can be attributed to different relative amounts of elemental and organic carbon (43), with biomass-burning aerosols containing a larger organic fraction and therefore having a larger absorption angstrom exponent than fossil fuel aerosols.

Fig. 1 illustrates the relationship between AAE1 and SAE1 for all AERONET measurements included in this study. Whereas the separation between dust-dominated and dust-free measurements based on the threshold values is clear, all fossil fuel and biomass-burning measurements occupy a continuous region of the phase space and the separation of pure EC and pure OC contributions requires additional analysis. Because EC has a weaker spectral dependence than OC, we can posit that the lower end of the AAE1 values reflects absorption due to EC. Fig. 2 illustrates the mean values of AAE1 calculated by averaging different fractions of the total frequency distribution at the different AERONET sites. We find that the mean AAE1 value asymptotically converges to 0.55 ± 0.24, representing the average low-end baseline for the absorption angstrom exponent. We relate this value to pure EC, again noting that varying amounts of co-occurring OC raise this value in ambient measurements. A similar analysis gives us a value of AAE2 = 0.83 ± 0.40 for EC. These values are found to be independent of the location, the source, and the total aerosol concentration and therefore can be considered robust representations of pure EC. Because both OC and dust have a stronger spectral dependence than EC, any observed values of AAE lower than these mean values correspond to BC-dominated aerosols, leading to our third constraint: If AAE1 < 0.55 and AAE2 < 0.83, AAOD = AAODEC.

The calculation of OC absorption angstrom exponents requires one additional assumption. Because OC absorbs primarily in the UV wavelength and at shorter visible (λ < 700 nm) wavelengths (13, 44), we modify Eq. **4** such that

$$\mathrm{AAOD_{OC}}(870) = 0. \qquad \textbf{[5]}$$

In dust-free regions the total AAOD at 870 nm is entirely due to EC, and the EC AAODs at 675 and 440 nm are calculated using Eq. **2**. Finally, Eq. **3** is used to calculate the OC AAODs at these two wavelengths, and the value of AAE1 for OC can be determined (because we assume OC does not absorb at 870 nm, AAE2 is undefined). The frequency distribution of OC AAE1 determined in this fashion is illustrated in Fig. 3 and is found to have a narrow distribution centered around 4.5 for all sites, further supporting our hypotheses that the absorption angstrom exponent is an intrinsic property. The mean value is found to be 4.55 ± 2.01.

Table 1 summarizes the values of absorption angstrom exponents determined in this work and compares them with the ranges of values reported in the literature, both based on measurements and determined from models using an assumed refractive index. The AAE values for dust and total carbon lie within the ranges reported in the literature and typically agree well with the central values. The AAE values for EC determined in this study are lower than literature values, and the values for OC lie toward the upper end reported in the literature. This indicates that EC and OC (treated as pure chemical species in this study) are typically comingled in combustion studies, even close to the source. Recent modeling studies have examined the effect of internal mixing between EC and OC on the AAE using a Mie-scattering algorithm in conjunction with a core-shell assumption (38, 45). OC coatings (representing internal mixing) are found to change the AAE for BC from 0.7 (no particles coated) to 0.1 (all particles coated), with this range being consistent with the value of 0.55 ± 0.24 calculated in this work. One final caveat needs to be considered in our approach: Any absorption by fine-mode dust (high

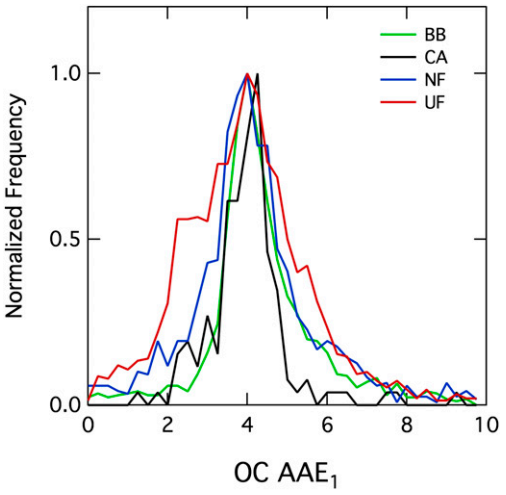

Fig. 3. Normalized frequency distribution of the OC absorption angstrom exponent determined from biomass burning (BB), California (CA), nonurban fossil fuel (NF), and urban fossil fuel (UF) sites between 440 and 675 nm.

Table 1. Absorption angstrom exponents for dust, total carbon, BC, and OC determined in this study and the ranges reported in the literature

	This work		Literature, measured		Literature, modeled	
Species	AAE1	AAE2	AAE	Refs.	AAE	Refs.
Dust	2.20 ± 0.50	1.15 ± 0.50	1.0–4.0	(22, 25, 50, 51)		
Total carbon	1.17 ± 0.40	1.23 ± 0.40	1.0–1.3	(19, 25, 52, 53)	1.0–1.7	(38)
BC/EC/soot	0.55 ± 0.24	0.85 ± 0.40	0.8–1.1	(35, 43)	1.00	(38)
OC	4.55 ± 2.01	—	1.8–7.0	(13, 19, 25, 35, 43, 54–56)	3.0–6.0	(28, 57)

AAE, high SAE) would be masked by absorption due to OC. Fig. 1*A* illustrates, however, that less than 1% of observations in regions with significant dust absorption lie in this phase space, consistent with most mineral dust being found in the coarse mode (46), and similarly less than 10% of points in the other regions fall in the coarse-dust region. We therefore do not expect significant errors due to fine-dust absorption.

Single Scattering Albedo

Whereas the total AAOD can be attributed to BC, OC, and dust using Eq. **4**, a similar partitioning of the AOD is not possible due to the variable contribution of purely scattering aerosols. To reconstruct the AOD for the absorbing species, we estimate the pure species single scattering albedo by a recursive numerical approach. The SSA is calculated at sites where each absorbing species is expected to be dominant; for example, BC SSA is determined only from fossil fuel-dominated sites. In summary, the derived SSAs for dust and OC (Fig. S2) are consistent with the range of values reported in the literature (Table S2) and both become more absorbing at shorter wavelengths. The spectral dependence of EC SSA on the other hand is weak and within the error at each bar at each wavelength; therefore, we use the value at 870 nm (with no OC and minimal dust absorption) for EC. We find a higher SSA for EC (0.38) than that typically reported by measurements (0.15–0.30). The published estimates are for aerosol particles generated in the laboratory or calculated in models (GOCART) whereas our SSA is based on ambient observations that are likely to reflect atmospherically processed EC that may have contamination from internally and/or externally mixed organics. This mixing will tend to enhance the aerosol SSA and therefore our SSA values should be considered as an upper limit. Our analysis constrains the EC SSA at 440 nm to values between 0.15 and 0.48, with an average value of 0.38. It should be noted that the derived SSA does not influence the absorption estimates because AAODs were derived independent of the SSAs.

California Case Study

With the complete set of AAE and SSA values, Eq. **4** with its associated constraints for dust-dominated, dust-free, and EC-dominated regimes can be applied to any set of multiwavelength absorption measurements. Here we apply this method to California, which provides an ideal test case due to varied aerosol emissions sources and readily available aerosol measurements and emission inventories. Although the CA AERONET dataset with valid SSA measurements is of insufficient size to construct a complete climatology, we can assess the seasonal and regional trends in aerosol properties and compare them to Goddard Chemistry, Aerosol, Radiation, and Transport (GOCART) model (29) predictions and regional emission estimates (47). The sensitivity of these results to the selected AAE parameterization is examined in Table S2. We define north-central California to be one region (north of 35 N) and southern California to be the other, such that both contain five operational AERONET sites, and the year is divided into two seasons: winter–spring from December to May and summer–fall from June to November. Table 2 summarizes the trends in AOD and AAOD for the absorbing species on the basis of the CA measurements and the GOCART model. Because SSA retrievals are valid only when the total AOD > 0.4 (42), comparing the absolute values results in a significant bias. We therefore report the AOD and AAOD fractions normalized by the total. In the seasonal comparison, we find that dust contributes a higher fraction of the AAOD in the winter–spring months (19% in northern California and 72% in southern California) compared with the summer–fall months (7% in northern California and 3% in southern California). Although the southern winter value may be anomalously high due to a few outliers, this general trend is consistent with trans-Pacific transport of dust seen in California in the winter months (48). We find a much higher absorption attributed to OC in the summer–fall months (27% in the north and 39% in the south) compared with the winter–spring months (15% in the north and 9% in the south), which is consistent with the California wildfires

Table 2. Dust, OC, and BC fraction of the total AAOD and AOD as determined from AERONET (this work) and the GOCART model in California

			This work 440 nm			GOCART 550 nm			This work 675 nm		
	Season	*n*	Dust	OC	BC	Dust	OC	BC	Dust	OC	BC
AAOD											
Northern and central California (>35 N)	December–May	77	0.19	0.15	0.66	0.51	0.11	0.38	0.12	0.03	0.84
	June–November	150	0.07	0.27	0.65	0.46	0.11	0.43	0.05	0.07	0.88
Southern California (<35 N)	December–May	35	0.72	0.09	0.18	0.50	0.10	0.40	0.64	0.03	0.33
	June–November	66	0.03	0.39	0.57	0.38	0.11	0.52	0.02	0.11	0.87
AOD											
Northern and central California (>35 N)	December–May	26	0.11	0.05	0.08	0.25	0.05	0.02	0.04	0.01	0.06
	June–November	87	0.05	0.11	0.10	0.23	0.05	0.02	0.02	0.01	0.09
Southern California (<35 N)	December–May	35	0.52	0.03	0.03	0.25	0.05	0.02	0.36	0.01	0.05
	June–November	66	0.01	0.14	0.07	0.19	0.05	0.03	0.01	0.03	0.12

associated with these months (49). BC makes up between 57% and 60% of the AAOD in all cases (Fig. S6), indicating that there are no seasonal or regional trends in California fossil fuel emissions. Regionally, dust comprises a higher fraction of the AAOD in northern California (consistent with transport events) and OC comprises a higher fraction in the south. The regional pattern may be an indication of absorption due to secondary organics that are typically present in high concentrations in the urban areas of southern California. We find good agreement in the OC fraction between our observationally constrained method and the GOCART predictions, with calculated values between 15% and 39% at 440 nm and 3% and 11% at 675 nm, bracketing the modeled fraction of 11% at 550 nm. We find a lower contribution and higher variability in the dust (7–72%) compared with those of GOCART, which attributes between 38% and 51% of AAOD to dust. One possible explanation for this difference is that the AERONET sites are primarily located along the coast and may not be sampling dust lofted from exposed lakebeds in inland California and the desert regions of Nevada and Arizona. Finally, we find that the three absorbing species compose between 16% and 52% of the total AOD, which is typically lower (except the anomalously high southern California winter value) than the 27–32% predicted by GOCART, indicating that the aerosol represented by AERONET measurements is more scattering. This difference can again be explained by the influence of the coastal sites that typically have a larger fraction of optical extinction due to purely scattering sea-salt and sulfate particles. The total AOD and AAOD (at 675 nm) for dust, EC, and OC are illustrated in Fig. 4 *A* and *B*, respectively: Although these are based on high pollution events, they still agree with the regional trends in emissions illustrated in Fig. 4*C*, indicating that our method provides a reasonable partitioning between the three species. Finally, Fig. 4*D* provides a unique wavelength-dependent perspective on the relative contribution of OC absorption: Although it is negligible at long wavelengths, it comprises up to 50% of the EC absorption at short wavelengths, indicating that the treatment of OC as being absorbing is critical for successful estimations of aerosol forcing. This result is consistent with measurements conducted in the Los Angeles basin that attributed between 25% and 30% of UV light absorption to organic carbon species and between 50% and 62% to black carbon particulates (17).

Conclusions

We have proposed an empirical method for determining the fraction of aerosol absorption attributable to dust, OC, and EC that exploits the differences in wavelength dependence for the principal absorbing species. We have self-consistently determined the AAE and SSA values associated with these species on the basis of a large global ensemble of AERONET measurements dominated by specific emission types. The parameter values are based entirely on observations and therefore do not require the assumption of aerosol chemical and physical properties such as refractive index, mixing state, or size distributions. These values are found to be consistent with those reported in the literature and in use in current aerosol models, in particular the AAE value for total carbon close to the theoretical value of 1.0. The method has been applied to California as a test case, where we find an enhanced absorption due to dust in the winter months and due to OC in the summer months. We find that OC on average contributes 28% to the total absorption at the shortest wavelength (440 nm), providing a good first-order estimate for the so-called brown carbon absorption that is presently poorly quantified.

We conclude by commenting on the general applicability of this method. Although we recommend values for the model

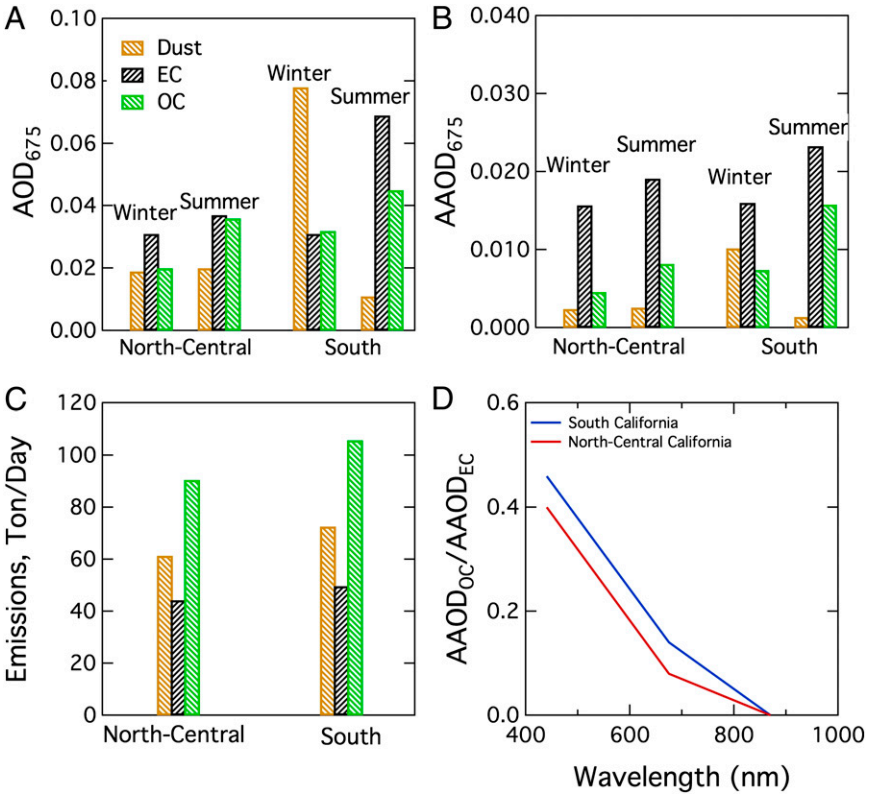

Fig. 4. (*A*–*C*) Species-resolved (*A*) AOD, (*B*) AAOD, and (*C*) emissions in California for EC, OC, and dust. (*D*) Wavelength-dependent relative absorption of OC and EC.

parameters based upon a global dataset, the equations can be fine tuned to any region by following the procedures outlined here for determining the SSA and AAE values. Because the only required input for the equation is a multiband measurement of the total absorption depth, the AERONET results reported here can be extended to the large ensembles of available diverse laboratory, ground-based, and remote satellite measurements. Finally, the analyses indicate the existence of significant BrC absorption that has been largely overlooked in climate models.

ACKNOWLEDGMENTS. This work was supported by the California Air Resources Board under contract 08-323 and the National Science Foundation under award ATM 0721142.

1. Andreae MO, Crutzen PJ (1997) Atmospheric aerosols: Biogeochemical sources and role in atmospheric chemistry. *Science* 276:1052–1058.
2. Bond TC, et al. (2007) Historical emissions of black and organic carbon aerosol from energy-related combustion, 1850-2000. *Global Biogeochem Cycles* 21:GB2018.
3. Yan F, Winijkul E, Jung S, Bond TC, Streets DG (2011) Global emission projections of particulate matter (PM): I. Exhaust emissions from on-road vehicles. *Atmos Environ* 45: 4830–4844.
4. Ramanathan V, Carmichael G (2008) Global and regional climate changes due to black carbon. *Nat Geosci* 1:221–227.
5. Ogren JA, Charlson RJ (1983) Elemental carbon in the atmosphere - cycle and lifetime. *Tellus B Chem Phys Meterol* 35:241–254.
6. Stier P, Seinfeld JH, Kinne S, Boucher O (2007) Aerosol absorption and radiative forcing. *Atmos Chem Phys* 7:5237–5261.
7. Jacobson MZ (2002) Control of fossil-fuel particulate black carbon and organic matter, possibly the most effective method of slowing global warming. *J Geophys Res Atmos* 107(D19):4410.
8. Jacobson MZ (2005) Corrections to "Control of fossil-fuel particulate black carbon and organic matter, possibly the most effective method of slowing global warming (vol 107, pg 4410, 2002)" *J Geophys Res Atmos* 110(D14):D14105.
9. Bahadur R, Feng Y, Russell LM, Ramanathan V (2011) Impact of California's air pollution laws on black carbon and their implications for direct radiative forcing. *Atmos Environ* 45:1162–1167.
10. Koch D, Bond TC, Streets D, Unger N, van der Werf GR (2007) Global impacts of aerosols from particular source regions and sectors. *J Geophys Res Atmos* 112(D2): D02205.
11. Myhre G, Hoyle CR, Berglen TF, Johnson BT, Haywood JM (2008) Modeling of the solar radiative impact of biomass burning aerosols during the Dust and Biomass-burning Experiment (DABEX). *J Geophys Res Atmos* 113:D00c16.
12. Chow JC, et al. (2009) Aerosol light absorption, black carbon, and elemental carbon at the Fresno Supersite, California. *Atmos Res* 93:874–887.
13. Kirchstetter TW, Novakov T, Hobbs PV (2004) Evidence that the spectral dependence of light absorption by aerosols is affected by organic carbon. *J Geophys Res Atmos* 109(D21):D21208.
14. Hoffer A, et al. (2006) Optical properties of humic-like substances (HULIS) in biomass-burning aerosols. *Atmos Chem Phys* 6:3563–3570.
15. Andreae MO, Gelencser A (2006) Black carbon or brown carbon? The nature of light-absorbing carbonaceous aerosols. *Atmos Chem Phys* 6:3131–3148.
16. Magi BI, Ginoux P, Ming Y, Ramaswamy V (2009) Evaluation of tropical and extra-tropical Southern Hemisphere African aerosol properties simulated by a climate model. *J Geophys Res Atmos* 114:D14204.
17. Jacobson MZ (1999) Isolating nitrated and aromatic aerosols and nitrated aromatic gases as sources of ultraviolet light absorption. *J Geophys Res Atmos* 104(D3): 3527–3542.
18. Alfaro SC, et al. (2004) Iron oxides and light absorption by pure desert dust: An experimental study. *J Geophys Res Atmos* 109(D8):D08108.
19. Bergstrom RW, et al. (2007) Spectral absorption properties of atmospheric aerosols. *Atmos Chem Phys* 7:5937–5943.
20. Bond TC, Bergstrom RW (2006) Light absorption by carbonaceous particles: An investigative review. *Aerosol Sci Technol* 40:27–67.
21. Clarke AD, et al. (2004) Size distributions and mixtures of dust and black carbon aerosol in Asian outflow: Physiochemistry and optical properties. *J Geophys Res Atmos* 109(D15):D15s09.
22. Fialho P, et al. (2006) The Aethalometer calibration and determination of iron concentration in dust aerosols. *J Aerosol Sci* 37:1497–1506.
23. Forster P, et al. (2007) Changes in atmospheric constituents and in radiative forcing. *Climate Change 2007: The Physical Science Basis. Contribution of Working Group I to the Fourth Assessment Report of the Intergovernmental Panel on Climate Change*, eds Solomon S, et al. (Cambridge Univ Press, New York).
24. Dubovik O, et al. (2002) Variability of absorption and optical properties of key aerosol types observed in worldwide locations. *J Atmos Sci* 59:590–608.
25. Russell PB, et al. (2010) Absorption Angstrom Exponent in AERONET and related data as an indicator of aerosol composition. *Atmos Chem Phys* 10:1155–1169.
26. Rizzo LV, Correia AL, Artaxo P, Procopio AS, Andreae MO (2011) Spectral dependence of aerosol light absorption over the Amazon Basin. *Atmos Chem Phys* 11:8899–8912.
27. Eck TF, et al. (1999) Wavelength dependence of the optical depth of biomass burning, urban, and desert dust aerosols. *J Geophys Res Atmos* 104(D24):31333–31349.
28. Arola A, et al. (2011) Inferring absorbing organic carbon content from AERONET data. *Atmos Chem Phys* 11:215–225.
29. Chin M, et al. (2009) Light absorption by pollution, dust, and biomass burning aerosols: A global model study and evaluation with AERONET measurements. *Ann Geophys* 27:3439–3464.
30. Park S-U, Chang L-S (2007) *Direct Radiative Forcing Due to Anthropogenic Aerosols in East Asia During 21–25 April 2001* (Springer, New York), pp 312–320.
31. Sato M, et al. (2003) Global atmospheric black carbon inferred from AERONET. *Proc Natl Acad Sci USA* 100(11):6319–6324.
32. Koven CD, Fung I (2006) Inferring dust composition from wavelength-dependent absorption in Aerosol Robotic Network (AERONET) data. *J Geophys Res Atmos* 111 (D14):D14205.
33. Dey S, Tripathi SN, Singh RP, Holben BN (2006) Retrieval of black carbon and specific absorption over Kanpur city, northern India during 2001-2003 using AERONET data. *Atmos Environ* 40:445–456.
34. Yang M, Howell SG, Zhuang J, Huebert BJ (2009) Attribution of aerosol light absorption to black carbon, brown carbon, and dust in China - interpretations of atmospheric measurements during EAST-AIRE. *Atmos Chem Phys* 9:2035–2050.
35. Sandradewi J, et al. (2008) Using aerosol light absorption measurements for the quantitative determination of wood burning and traffic emission contributions to particulate matter. *Environ Sci Technol* 42(9):3316–3323.
36. Chung CE, Ramanathan V, Decremer D (2012) Observationally constrained estimates of carbonaceous aerosol radiative forcing. *Proc Natl Acad Sci USA* 109(29): 11624–11629.
37. Flowers BA, et al. (2010) Optical-chemical-microphysical relationships and closure studies for mixed carbonaceous aerosols observed at Jeju Island; 3-laser photoacoustic spectrometer, particle sizing, and filter analysis. *Atmos Chem Phys* 10:10387–10398.
38. Gyawali M, Arnott WP, Lewis K, Moosmuller H (2009) In situ aerosol optics in Reno, NV, USA during and after the summer 2008 California wildfires and the influence of absorbing and non-absorbing organic coatings on spectral light absorption. *Atmos Chem Phys* 9:8007–8015.
39. Moosmuller H, Chakrabarty RK, Ehlers KM, Arnott WP (2011) Absorption Angstrom coefficient, brown carbon, and aerosols: Basic concepts, bulk matter, and spherical particles. *Atmos Chem Phys* 11:1217–1225.
40. Horvath H, Noll KE (1969) Relationship between atmospheric light scattering coefficient and visibility. *Atmos Environ* 3:543–552.
41. Holben BN, et al. (2001) An emerging ground-based aerosol climatology: Aerosol optical depth from AERONET. *J Geophys Res Atmos* 106(D11):12067–12097.
42. Dubovik O, King MD (2000) A flexible inversion algorithm for retrieval of aerosol optical properties from Sun and sky radiance measurements. *J Geophys Res Atmos* 105(D16):20673–20696.
43. Levin EJT, et al. (2010) Biomass burning smoke aerosol properties measured during Fire Laboratory at Missoula Experiments (FLAME). *J Geophys Res Atmos* 115:D182010.
44. Laskin J, et al. (2010) High-resolution desorption electrospray ionization mass spectrometry for chemical characterization of organic aerosols. *Anal Chem* 82(5): 2048–2058.
45. Chung CE, Lee K, Muller D (2012) Effect of internal mixture on black carbon radiative forcing. *Tellus B Chem Phys Meterol* 64:1–13.
46. Kim D, et al. (2011) Dust optical properties over North Africa and Arabian Peninsula derived from the AERONET dataset. *Atmos Chem Phys* 11:10733–10741.
47. CARB (2008) Emission inventory data. Available at http://www.arb.ca.gov/ei/emissiondata.htm. Accessed July 14, 2012.
48. Hadley OL, et al. (2007) Trans-Pacific transport of black carbon and fine aerosols (D < 2.5 mu m) into North America. *J Geophys ResAtmos*, 112: D05309.
49. Westerling AL, Hidalgo HG, Cayan DR, Swetnam TW (2006) Warming and earlier spring increase western U.S. forest wildfire activity. *Science* 313(5789):940–943.
50. Coen MC, et al. (2004) Saharan dust events at the Jungfraujoch: Detection by wavelength dependence of the single scattering albedo and first climatology analysis. *Atmos Chem Phys* 4:2465–2480.
51. Weinzierl B, et al. (2011) Microphysical and optical properties of dust and tropical biomass burning aerosol layers in the Cape Verde region-an overview of the airborne in situ and lidar measurements during SAMUM-2. *Tellus B Chem Phys Meterol* 63: 589–618.
52. Schnaiter M, et al. (2003) UV-VIS-NIR spectral optical properties of soot and soot-containing aerosols. *J Aerosol Sci* 34:1421–1444.
53. Virkkula A, et al. (2005) Modification, calibration and a field test of an instrument for measuring light absorption by particles. *Aerosol Sci Technol* 39:68–83.
54. Clarke A, et al. (2007) Biomass burning and pollution aerosol over North America: Organic components and their influence on spectral optical properties and humidification response. *J Geophys Res. Atmos* 112(D12):D15s09.
55. Schnaiter M, et al. (2006) Strong spectral dependence of light absorption by organic carbon particles formed by propane combustion. *Atmos Chem Phys* 6:2981–2990.
56. Schnaiter M, et al. (2005) Measurement of wavelength-resolved light absorption by aerosols utilizing a UV-VIS extinction cell. *Aerosol Sci Technol* 39:249–260.
57. Sun HL, Biedermann L, Bond TC (2007) Color of brown carbon: A model for ultraviolet and visible light absorption by organic carbon aerosol. *Geophys Res Lett* 34:L17813.

Supporting Information

Bahadur et al. 10.1073/pnas.1205910109

SI Text

Aerosol Robotic Network. The ground-based Aerosol Robotic Network (AERONET), a globally distributed network of automated sun and sky radiometers (1), provides long-term, continuous, and readily available measurements of aerosol optical properties that are an ideal resource for this study. In addition to multiband retrievals of aerosol optical depth (AOD) between 340 and 1020 nm from direct sun measurements, the inversion algorithm provides single scattering albedo (SSA) [and corresponding absorption aerosol optical depth (AAOD)] estimates from sky radiance measurements at 440, 675, 870, and 1020 nm (2). Several AERONET sites are dominated by emissions corresponding to a single absorbing aerosol (3). To parameterize Eq. **4** with absorption angstrom exponent (AAE) values for elemental carbon (EC), we use fossil fuel-dominated sites separated into urban and nonurban regions. Similarly, we use biomass-burning–dominated sites to parameterize organic carbon/brown carbon (OC/BrC)- and dust-dominated sites for dust. Table S1 provides the details of the sites selected for this analysis sorted into regions dominated by dust (DU), biomass burning (BB), urban fossil-fuel (UF), nonurban fossil-fuel (NF) emissions; and geographically in the state of California (CA). We use the daily average quality-assured data (designated as Version 2, Level 2.0) in this work. This limits the total number of valid SSA (and corresponding AAOD) retrievals; however, there are significant data for the results to be statistically significant.

Dust Absorption Angstrom Exponent. Because dust and carbonaceous aerosols have distinct sources and differing chemical and physical properties (3), the determination of dust absorption characteristics is the first logical step in our analysis. However, ambient dust is often mixed with anthropogenic and biogenic pollution even at desert sites (and conversely, combustion-dominated sites show influence of dust) (4) and the entire dataset of measurements from dust dominated (DU) sites (Table S1) cannot be used to determine properties for pure dust. Compared with combustion aerosols that are predominantly in the fine (submicron) mode close to sources, dust particles are dominated by coarse (supermicron) mode particles that have a weak spectral dependence for the total extinction (5). At the same time, dust particles absorb more strongly at shorter wavelengths, so we can establish thresholds in AAE1 and scattering angstrom exponent SAE1 for identifying dust-dominated (and dust-free) measurements (3). Fig. S1*A* shows the normalized probability distribution of SAE1 determined from the AERONET data summarized in Table S1. We find a clear separation between the DU and biomass-burning (BB)/urban- and nonurban-sites fossil fuel (UF + NF) measurements. A threshold value of 0.5 in SAE1 results in a good separation, with 76% of DU measurements satisfying the condition extinction angstrom exponent (EAE)1 < 0.5, compared with only 1% of BB/FF measurements. Fig. S1*B* shows a larger overlap when only AAE1 is considered, with 72% of DU measurements and 17% of BB/FF measurements satisfying the condition AAE1 > 1.5. The AAE2 overlap for all datasets (Fig. S1*C*), and there appears to be a separation when the AAE2/AAE1 ratio is considered (Fig. S1*D*). Due to the existing overlaps in any one of these frequency distributions, we use a dual threshold to rigorously identify dust-dominated measurements: SAE1 < 0.5 and (AAE1 > 1.5 or AAE2/AAE1 < 0.4). This condition is satisfied by 66% of the DU points and less than 0.5% of BB/FF points. We calculate the angstrom exponents for pure dust by averaging these measurements and find AAE1 = 2.20 ± 0.50 and AAE2 = 1.15 ± 0.40.

We follow a similar procedure for establishing threshold values for identifying dust-free (alternatively, carbon-dominated) measurements. We select the conditions SAE1 > 1.2 or AAE2/AAE1 > 0.8 that are satisfied by 97% of all BB/FF measurements and 18% of the DU measurements. The mean values for AAE1 calculated from dust-free measurements for absorption due to total carbon are 1.06 (FF), 1.14 [nonurban fossil fuel (NF)], and 1.28 (BB), agreeing well with the value of 1.0 typically reported for black carbon (6).

Sensitivity to AAE. Due to the exponential nature of Eq. **4**, it is possible that the choice of AAE for the three absorbing species may have a significant impact on the AAOD partition. Using the California AERONET data as a comparative case study, we recalculate the AAOD for dust, OC (BrC), and black carbon (BC), using the extreme values of AAE reported in Table 1 to determine the sensitivity of the partitioning method to the parameterization. The results are summarized in Table S2 at 440 nm. For the various cases, we still find that BC is the primary absorber (except when we select the low extreme value for both the BC and the OC AAE), contributing about 45% of the total AAOD, with dust and OC making up the remainder. The partitioning for dust is most stable, with dust AAOD varying between 0.005 and 0.011, and the highest variability is found in OC absorption, with the AAOD varying between 0.000 (negligible) and 0.014. This result is consistent with the SAE-AAE phase space we have defined, because dust absorption is clearly separated, whereas OC/BC partitioning is less defined.

Calculating Single Scattering Albedo. To fully parameterize our partitioning method, we need to determine the SSA for the three pure components. Unlike the AAE, the SSA cannot be determined from a simple average of observations because each measurement is influenced by (an unknown amount of) comingled scattering species such as sulfates or nitrates. Instead, using an ensemble of measurements we try to locate the limiting case via extrapolation where the influence of scattering aerosols is negligible, and the SSA may be therefore be attributed to the absorbing species only. To determine this limit mathematically, we first need to establish a linear relationship between the SSA and AOD. In a mixture of an absorbing aerosol A and nonabsorbing aerosol N, the scattering optical depth, SAOD, and the absorption optical depth, AAOD, can be written as

$$\mathrm{SAOD} = \mathrm{SAOD_A} + \mathrm{SAOD_N} \qquad \textbf{[S1]}$$

$$\mathrm{AAOD} = \mathrm{AAOD_A} + \mathrm{AAOD_N}. \qquad \textbf{[S2]}$$

Furthermore, because SSA = SAOD/(SAOD + AAOD), we can rewrite the above equations as

$$(\mathrm{SSA})\mathrm{AOD} = (\mathrm{SSA_A})\mathrm{AOD_A} + (\mathrm{SSA_N})\mathrm{AOD_N} \qquad \textbf{[S1a]}$$

$$(1-\mathrm{SSA})\mathrm{AOD} = (1-\mathrm{SSA_A})\mathrm{AOD_A} + (1-\mathrm{SSA_N})\mathrm{AOD_N}. \qquad \textbf{[S2a]}$$

Realizing that $\mathrm{SSA_N} = 1$, the ratio of the two equations yields

$$\mathrm{SSA}/(1-\mathrm{SSA}) = \mathrm{SSA_A}/(1-\mathrm{SSA_A}) + k(\mathrm{AOD}-\mathrm{AOD_A})/\mathrm{AOD_A}, \quad \textbf{[S3]}$$

where $k = 1/(1 - \mathrm{SSA_A})$ and the limit of $\mathrm{AOD} = \mathrm{AOD_A}$ represents the point where the aerosol consists entirely of a single absorbing species (the limit of interest). The advantage of formulating the AOD as a difference in this manner is that this 0 limit allows us to mathematically isolate the contributions from a single absorbing species (such as EC or BrC) whereas all absorbing species coexist to a certain degree even in emissions dominated by a single species. The pure component SSA can be calculated by applying Eq. **S3** to sets of observations likely to be dominated by a single absorbing species to minimize deviation from the limit of $\mathrm{AOD} - \mathrm{AOD_A} = 0$; i.e., BC SSA is determined from the fossil fuel-burning stations in Table S1, OC SSA is determined from the biomass-burning stations, and dust SSA is determined from the dust-dominated stations. As written, Eq. **S3** cannot be directly solved because it contains two unknowns, $\mathrm{SSA_A}$ and $\mathrm{AOD_A}$, with SSA and AOD composing the ensemble of observations. Instead, we determine $\mathrm{SSA_A}$ recursively, using a least-squares regression with an assumed value of $\mathrm{SSA_A}$ applied to Eq. **S3**, treating observed $\mathrm{SSA}/(1 - \mathrm{SSA})$ as the y (dependent) variable and $(\mathrm{AOD} - \mathrm{AOD_A})/\mathrm{AOD_A}$ as the x (independent) variable. For a given set of observations, values of SSA and $\mathrm{AAOD_A}$ (based on our partition scheme) are known. We then assume a (initial) value of $\mathrm{SSA_A}$ from the literature (Table S3), allowing us to calculate $\mathrm{AOD_A}$ and (recursively) determine the y-intercept (corresponding to the limit of absorption by a single species), and recalculate a new value of $\mathrm{SSA_A}$ that is then treated as the new "assumed' value, and then the process is repeated. When the assumed and calculated SSA values agree within a tolerance of 10%, we consider the solution to have converged.

Fig. S2 illustrates the SSA (at 675 nm) calculated for EC, OC, and dust, using AERONET sites grouped by region. We find similar values among the different regions, indicating that similar to the AAE, the SSA appears to be an intrinsic chemical property largely independent of the emission source and region. The corresponding wavelength dependence is summarized in Table S3, which also shows the range of corresponding measured values and those currently used in the Goddard Chemistry, Aerosol, Radiation, and Transport (GOCART) model.

Concentration Independence of Intrinsic Properties. A limitation of the AERONET dataset used to tune the equations in this work is that SSA retrievals are valid only when the AOD (440 nm) > 0.4, i.e., high pollution events. This raises the possibility that the intrinsic properties we calculate—the AAE and the SSA—may be biased and not universal for dust, EC, and OC. Fig. S3 illustrates the measured SSA and calculated AAE1 as a function of the measured AOD for the AERONET sites listed in Table S1. We find that the AAE is independent of the measured AOD and that the biomass sites have the largest AAE, consistent with a higher absorbing OC fraction at these sites, whereas the North American urban sites have the lowest AAE, again consistent with a larger EC fraction.

Similarly, the scatter plot shows the independence of SSA relative to the AOD, although all measurements with SSA correspond to high pollution events; i.e., AOD > 0.4. We find that SSA at 675 nm is generally higher than SSA at 440 nm; this is consistent with aerosols becoming less absorbing at longer wavelengths, i.e., loss of absorption due to OC and dust. These scatter plots suggests that there is no bias in the AERONET for the SSA and AAE measurements.

In addition to regional averages, we have also examined the dependence of AAE and SSA on the AOD at individual AERONET sites to isolate any bias. Again, we find that these properties are independent of the total aerosol depth (Fig. S4) and are likely a function only of the mixing state of the aerosols.

Error Estimation in Method. Fig. S5 illustrates the AAOD reconstructed from Eq. **4** compared with the AERONET measured value using 675 nm as the reference wavelength. The discrepancy in values corresponds to the error introduced by the partitioning method. We find that at 440 nm the AAOD is overestimated by 0.5% on average, and at 870 nm the AAOD is underestimated by 4.0%. Negative values of AAOD for at least one of the species are predicted for 27 of the 342 measurements (7%); these values are excluded from determining ensemble averages. These relatively small values of error indicate that the method based upon a set of global measurements is fairly robust and applicable even at the regional scale.

Overall, we find that the partitioning scheme reproduces between 95% and 100% of the measured AAOD at all wavelengths and produces nonphysical results for ~8% of all measurements. However, we contend that these uncertainties are not unreasonably large, and the method reproduces seasonal and regional trends that are consistent with observed emission patterns.

Relative Absorption by EC, OC, and Dust. Fig. S6 illustrates the relative contributions of dust, OC, and EC to the AAOD at 440 nm in California. We find that dust is the weakest absorber in California, but also has the highest variability, with a mean AAOD of 0.005 ± 0.018. OC comprises the next highest fraction, with a mean AAOD of 0.009 ± 0.014, and EC has an average AAOD of 0.018 ± 0.012. The average contributions to the total AAOD are 15% (dust), 28% (OC), and 56% (EC). Finally, only measurements with a high AAE/low EAE have significant dust absorption, and correspondingly measurements with high AAE/high EAE have significant OC absorption, with BC absorption being predominant at low AAE values. These trends are consistent with those expected for dust, biomass burning, and fossil fuel aerosols, respectively (3).

1. Holben BN, et al. (2001) An emerging ground-based aerosol climatology: Aerosol optical depth from AERONET. *J Geophys Res Atmos* 106(D11):12067–12097.
2. Dubovik O, King MD (2000) A flexible inversion algorithm for retrieval of aerosol optical properties from sun and sky radiance measurements. *J Geophys Res Atmos* 105 (D16):20673–20696.
3. Russell PB, et al. (2010) Absorption Angstrom Exponent in AERONET and related data as an indicator of aerosol composition. *Atmos Chem Phys* 10:1155–1169.
4. Eck TF, et al. (2010) Climatological aspects of the optical properties of fine/coarse mode aerosol mixtures. *J Geophys Res Atmos* 115:D19205.
5. Kim D, et al. (2011) Dust optical properties over North Africa and Arabian Peninsula derived from the AERONET dataset. *Atmos Chem Phys* 11:10733–10741.
6. Bond TC, Bergstrom RW (2006) Light absorption by carbonaceous particles: An investigative review. *Aerosol Sci Technol* 40:27–67.

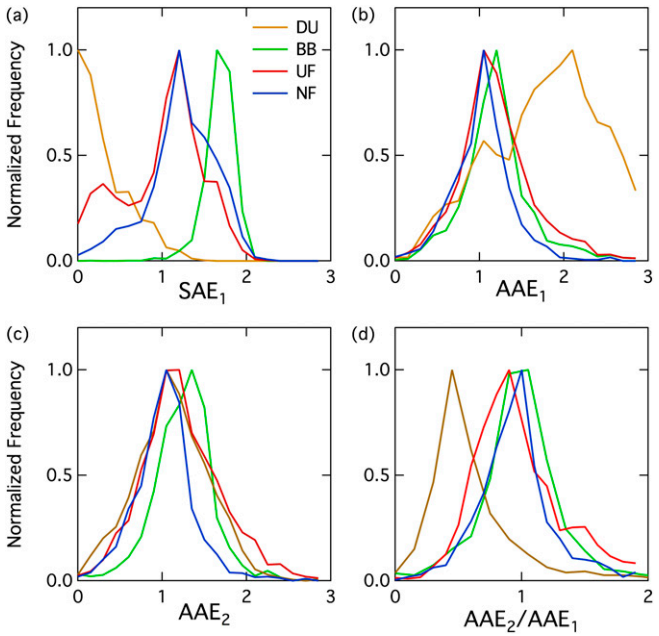

Fig. S1. (*A*–*D*) Normalized frequency distributions for the (*A*) scattering angstrom exponent (440–675 nm); (*B*) absorption angstrom exponent (440–675 nm); (*C*) absorption angstrom exponent (675–870 nm); and (*D*) AAE2/AAE1 ratio measured at DU (brown), BB (green), UF (red), and NF (blue) AERONET sites listed in Table S1.

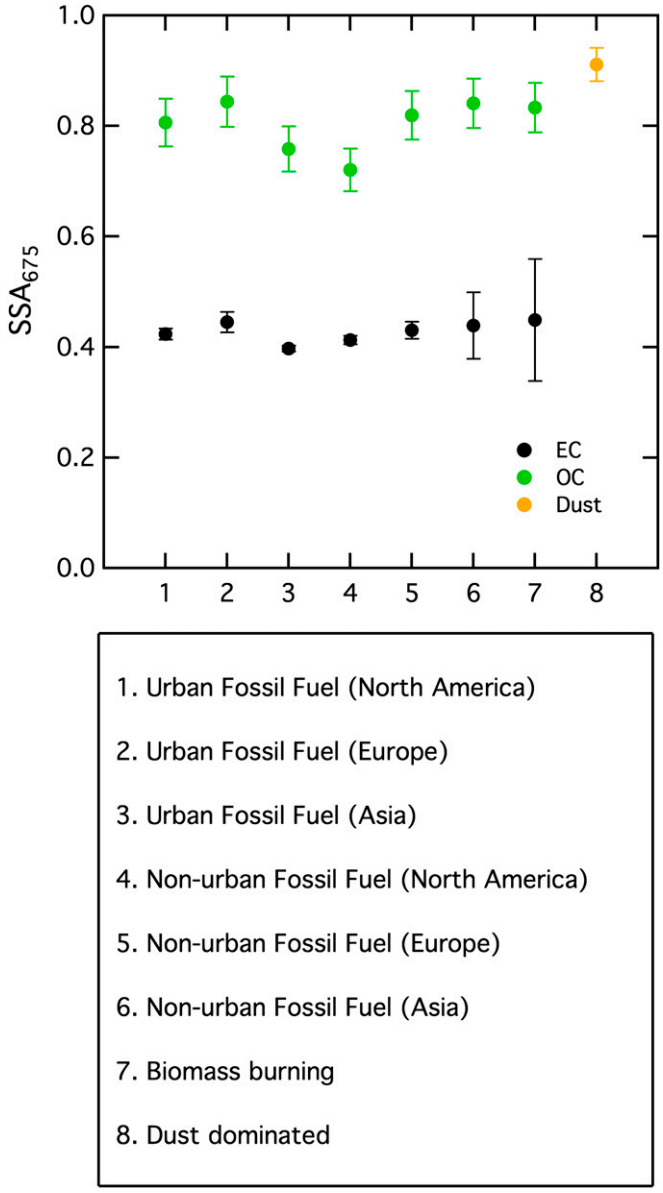

Fig. S2. Calculated SSA value at 675 nm for EC, OC, and dust, using AERONET stations segregated into source regions as described in Table 1.

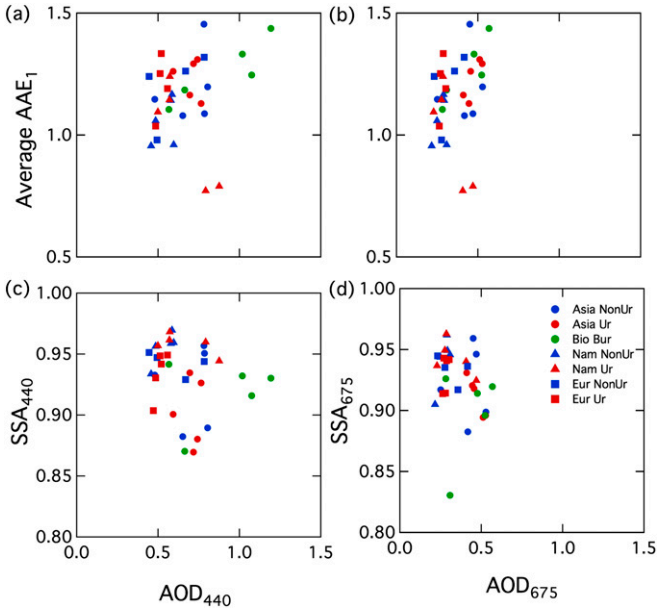

Fig. S3. (*A*–*D*) The calculated AAE1 for the total aerosol as a function of AOD at (*A*) 440 nm and (*B*) 675 nm and the measured SSA at (*C*) 440 nm and (*D*) 675 nm from AERONET sites listed in Table S1.

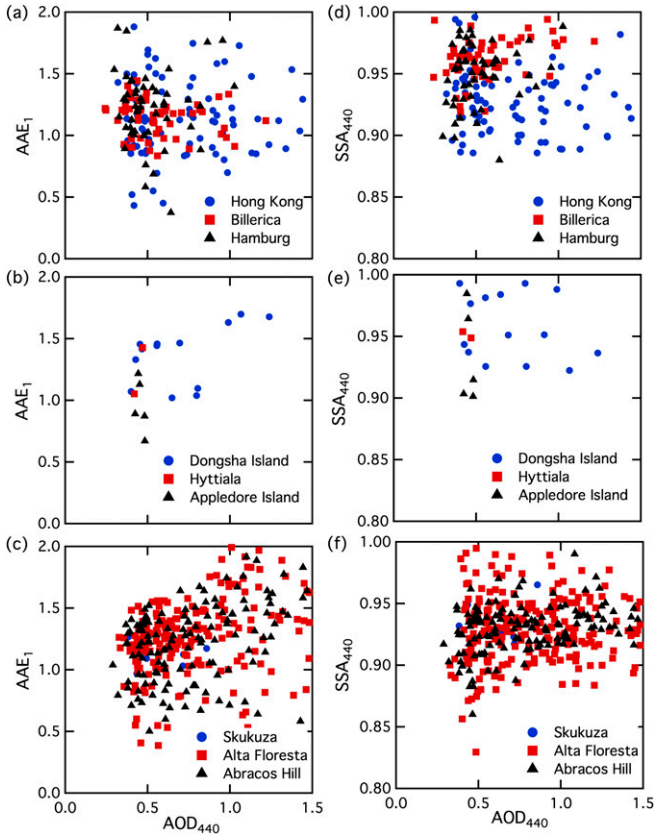

Fig. S4. (*A*–*C*) Calculated AAE1 for the total aerosol as a function of AOD at 440 nm. (*D*–*F*) Measured SSA at 440 nm from selected AERONET sites listed in Table S1.

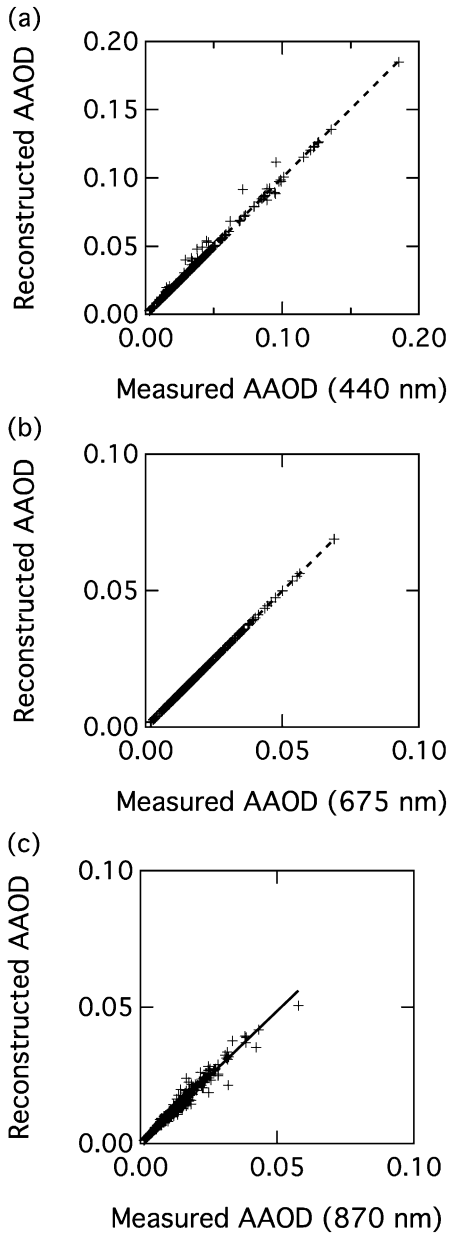

Fig. S5. (*A*–*C*) Comparison of AAOD from CA sites measured from AERONET and reconstructed from Eq. **4** at (*A*) 440 nm, (*B*) 675 nm, and (*C*) 870 nm.

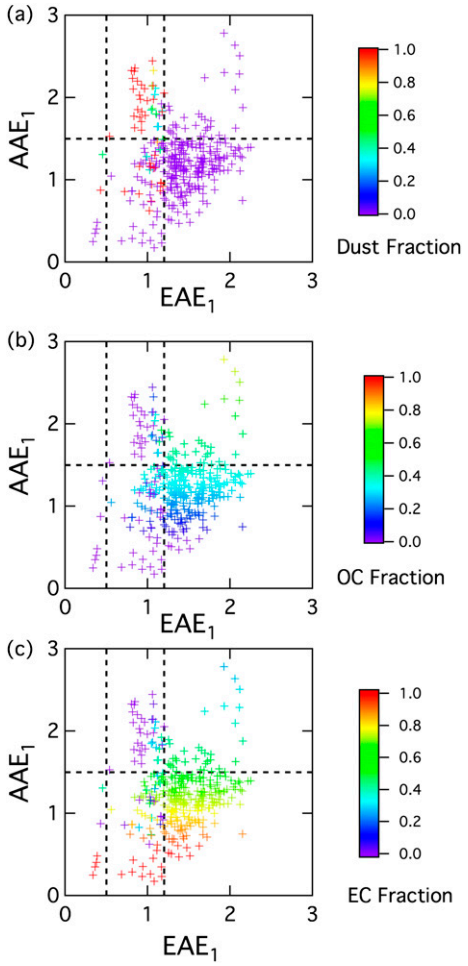

Fig. S6. (*A*–*C*) Fraction of AAOD in CA attributed to (*A*) dust, (*B*) OC, and (*C*) EC at 440 nm.

Table S1. AERONET sites used to obtain AOD and AAOD measurements

Group	Dominant emission source	Sites	Valid SSA retrievals	Reference
DU	Dust	Tamanrasset (Algeria), Solar Village (Saudi Arabia), Hamim (United Arab Emirates), Eilat (Israel)	1,312	(1)
BB	Biomass burning	Abracos Hill (Brazil), Alta Floresta (Brazil), Belterra (Brazil), Campo Grande (Brazil), Petrolina (Brazil), Rio Branco (Brazil), Mongu (Zambia), Skukuza (South Africa)	1,452	(2, 3)
UF	Urban sites, fossil fuel combustion	Billerica (MA, USA), City College of New York (NY, USA), Fresno (CA, USA), Goddard Space Flight Center (MD, USA), Halifax (Canada), MD Science Center (MD, USA), Hamburg (Germany), Institute for Tropospheric Research Leipzig (Germany), Istituto per lo Studio delle Dinamica delle Grandi Masse (Italy), Mainz (Germany), Palaiseau (France), Rome (Italy), Hong Kong (China), Karachi (Pakistan), New Delhi (India), Taipei Central Weather Bureau (Taiwan), Kanpur (India)	2,105	(4)
NF	Nonurban sites, fossil fuel and mixed sources	Appledore Island (NH, USA), Bondville (IL, USA), Sioux Falls (SD, USA), Walker Branch (MI, USA), Cleveland Area Rapid Transit Oklahoma (OK, USA), Hyttiala (Finland), Tenerife (Spain), Toravere (Estonia), Villefranche (France), Dongsha Island (China), Gandhi College (India), Pantnagar (India), Xanthi (China)	1,385	(4)
CA	Mixed (all in California)	Fresno, La Jolla, Jet Propulsion Laboratory, Monterey, Moss Landing, San Nicholas, Table Mountain, Trinidad Head, University of California Los Angeles, University of California Santa Barbara	342	

1. Kim D, et al. (2011) Dust optical properties over North Africa and Arabian Peninsula derived from the AERONET dataset. *Atmos Chem Phys* 11:10733–10741.
2. Hoelzemann JJ, et al. (2009) Regional representativity of AERONET observation sites during the biomass burning season in South America determined by correlation studies with MODIS Aerosol Optical Depth. *J Geophys Res Atmos* 114:D13301.
3. Magi BI, Ginoux P, Ming Y, Ramaswamy V (2009) Evaluation of tropical and extratropical Southern Hemisphere African aerosol properties simulated by a climate model. *J Geophys Res Atmos* 114:D14204.
4. Xia XG, Eck TF, Holben BN, Phillippe G, Chen HB (2008) Analysis of the weekly cycle of aerosol optical depth using AERONET and MODIS data. *J Geophys Res Atmos* 113(D14):D14217.

Table S2. Sensitivity of AAOD partitioning to choice of AAE for the California case study

Perturbation	Dust	OC	BC
California AAOD at 440 nm			
Base conditions (AAE values listed in Table 1)	0.009	0.007	0.017
BC AAE1 = 0.79, AAE2 = 1.25	0.008	0.005	0.020
BC AAE1 = 0.31, AAE2 = 0.45	0.008	0.009	0.016
OC AAE1 = 6.56	0.005	0.000	0.028
OC AAE1 = 2.54	0.007	0.012	0.014
BC AAE1 = 0.79, OC AAE1 = 6.56	0.011	0.003	0.019
BC AAE1 = 0.31, OC AAE1 = 2.54	0.007	0.014	0.012
Dust AAE1 = 1.70, AAE2 = 0.65	0.006	0.009	0.018
Dust AAE1 = 2.70, AAE2 = 1.65	0.011	0.005	0.017

Table S3. Wavelength-dependent single scattering albedo determined in this work compared with literature values

	SSA, this work			SSA, measured		SSA, GOCART	
	440 nm	675 nm	870 nm	550 nm	Ref.	550 nm	Ref.
BC	0.480	0.428	0.386	0.15–0.30	(1–4)	0.20–0.50	(5)
OC	0.772	0.801	1.000	0.85–0.95	(2, 6, 7)	0.90–1.00	(5)
Dust	0.870	0.901	0.941	0.90–0.95	(6–8)	0.60–0.90	(5)

1. Bond TC, Bergstrom RW (2006) Light absorption by carbonaceous particles: An investigative review. *Aerosol Sci Technol* 40:27–67.
2. Magi BI, Ginoux P, Ming Y, Ramaswamy V (2009) Evaluation of tropical and extratropical Southern Hemisphere African aerosol properties simulated by a climate model. *J Geophys Res Atmos* 114:D14204.
3. Koylu UO, Faeth GM (1994) Optical properties of overfire soot in buoyant turbulent diffusion flames at long residence times. *Trans ASME J Heat Transfer* 116:152–159.
4. Schnaiter M, et al. (2003) UV-VIS-NIR spectral optical properties of soot and soot-containing aerosols. *J Aerosol Sci* 34:1421–1444.
5. Chin M, et al. (2009) Light absorption by pollution, dust, and biomass burning aerosols: A global model study and evaluation with AERONET measurements. *Ann Geophys* 27: 3439–3464.
6. Russell PB, et al. (2010) Absorption Angstrom Exponent in AERONET and related data as an indicator of aerosol composition. *Atmos Chem Phys* 10:1155–1169.
7. Bergstrom RW, et al. (2007) Spectral absorption properties of atmospheric aerosols. *Atmos Chem Phys* 7:5937–5943.
8. Wolff MJ, et al. (2009) Wavelength dependence of dust aerosol single scattering albedo as observed by the Compact Reconnaissance Imaging Spectrometer. *J Geophys Res Planets* 114: E00D04.